IEEE Access
Multidisciplinary ⋮ Rapid Review ⋮ Open Access Journal

Received March 8, 2021, accepted April 9, 2021, date of publication April 21, 2021, date of current version May 3, 2021.

Digital Object Identifier 10.1109/ACCESS.2021.3074696

Modelling and Nonlinear Control of a Magnetically Coupled Multiport DC-DC Converter for Automotive Applications

VICTOR REPECHO, JOSEP M. OLM, ROBERT GRIÑÓ, (Senior Member, IEEE), ARNAU DÒRIA-CEREZO, AND ENRIC FOSSAS, (Senior Member, IEEE)
Institute of Industrial and Control Engineering, Universitat Politècnica de Catalunya, 08028 Barcelona, Spain

Corresponding author: Victor Repecho (victor.repecho.del@upc.edu)

This work was supported in part by the Government of Spain through the Agencia Estatal de Investigación under Project DPI2017-85404-P, and in part by the Generalitat de Catalunya through the Agència de Gestió d'Ajuts Universitaris i de Recerca (AGAUR) Project under Grant 2017 SGR 872.

ABSTRACT This work presents a nonlinear control strategy for a magnetically coupled multiport dc-dc converter aimed at automotive applications. First, a behavioural dynamic model, based on averaging the power flowing among the ports, is derived. Then, a control algorithm, based on feedback linearization techniques, is proposed. Essentially, the controller ensures decoupling and a linear dynamic behaviour thanks to a transformation of control and state variables, and a conventional PI action is devised to render asymptotic stability, as well as robustness to load uncertainties. The inversion of the control transformation, which involves nonlinear terms, is carried out using linear approximations with no significant performance decay. Hence, simplicity and efficiency are the main features of the control design. The proposed controller is validated via experimental results.

INDEX TERMS Isolated multiport dc-dc converter, bidirectional power flow, nonlinear control, feedback linearization, decoupling, phase-shifted pulse width modulation, automotive applications.

I. INTRODUCTION

In the last years two main challenges have araisen in the automotive sector: on the one hand we have CO_2 reduction, which implies a weight reduction and an efficiency increase of the vehicle components [1]; on the other hand we have the customer's requirements, mainly in terms of performance and security. Consequently, the use of electrified systems has emerged as an alternative to be taken into account by OEMs (Original Equipment Manufacturers). This new tendency does not only consider the electrification of the power train (i.e. electrical and hybrid vehicles), but it is also evident in many auxiliary devices that are increasingly being electrified [2].

However, a major electrification of vehicles entails issues related to on-board dc micro-grids. This implies the necessity of designing: (i) controllers ensuring grid stability in the face of the connection of constant power loads (CPLs), as well as good robustness and efficiency properties, and (ii) optimization algorithms for the dc micro-grid.

The associate editor coordinating the review of this manuscript and approving it for publication was Cheng Qian.

This paper considers a dc multi-bus architecture with the most used voltages in automotive applications, namely, 400 V for the power train [3], [4], and 48 V and 12 V, for auxiliary devices, composed by only one storage element (batteries), see Figure 1. The main advantage of using only one battery and one power converter is size and weight reduction.

The dc buses are connected by a magnetically coupled multiport dc-dc converter. Magnetically-based converters have been used not only for electrical vehicles [5], but also for connecting different dc networks in traction systems [6], electric aircrafts [7], [8], satellites [9], energy management systems [10], [11], dc grids [12], interfacing different solar photovoltaic modules [13], or MTDC transmission system [14]. The attractiveness of this topology is, among others, related to the use of less components (because switching devices and storage elements are shared) resulting in lower overall mass and compact packaging, power flow bidirectionality in each port, and galvanic isolation among different dc networks thanks to the magnetic core. Several topologies have been proposed for multiport converters: fully electrically isolated configurations, with a separate winding in each port, include single magnetic

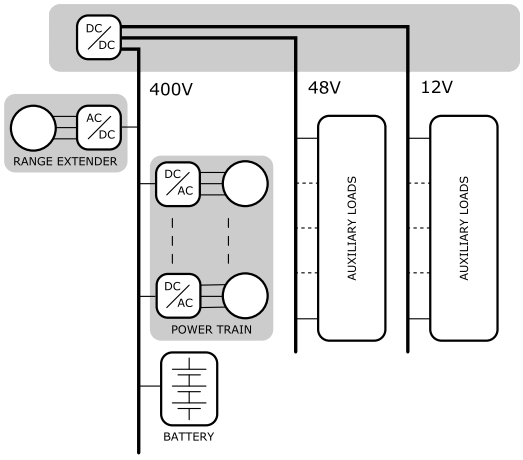

FIGURE 1. DC multi-bus system for automotive applications.

core [15], [16], a derived delta-type model for three-winding transformer [17], or dual-transformer topologies [18]. Other schemes reduce the number of windings (and, consequently, the size and weight), see [19]. In automotive applications, due to safety considerations, a fully isolated scheme is the preferred topology.

A. MODELLING APPROACHES

The multi-port dc-dc converter results in a non-linear dynamical system that mixes the dc stages at the dc buses with an ac stage in between due to the magnetic transformer. This prevents the adoption of the equivalent circuit model to design control strategies and requires the modification of the model. One alternative is the use of averaging methods such as the generalized state-space averaging (GSSA) technique. The GSSA methodology was proposed for a dual-active bridge (DAB) converter in [20], and later extended in [21]. See also [22] for a three-phase DAB converter. The main attractiveness of using such Fourier harmonic approach is that the resulting model provides a good physical insight.

Other alternatives can be found in the literature, such as the generalized input impedance model [23]. However, the behavioural model obtained from averaging the power flow among different ports is the most used approach. The exact derivation of this model has been reported in [24] assuming a periodic regime of voltages and currents in the high frequency transformer. The result is a nonlinear system with order equal to the number of dc buses.

B. CONTROL OF DC-DC MULTIPORT CONVERTERS

Usually, the control of magnetically coupled dc-dc converters is achieved by means of a high frequency square signal, where the control input is the phase-shift applied to each port. With this strategy and, under some conditions, soft-switching can be achieved [25]. Most of the papers propose classical PI controllers [7], [13], [18], [26], some of them with small variations for better transient behaviours, such as feed-forward terms [6], [27] or inner current loops [11].

Alternatively, other linear approaches can be found in the literature, including decoupling methods [19], [28], [29], compensators [30], [31], optimal Linear Quadratic Gaussian control [32], or H_∞ control [33]. The aforementioned control strategies are based on linearized models and the analysis is based on small-gain approximations. Only few papers propose nonlinear strategies such as passivity-based controllers [34], [35] or adaptive algorithms [36].

C. CONTRIBUTION AND PAPER ORGANIZATION

The aim of this paper is to develop a feedback linearization-based control strategy for a dc multi-bus and a multiport power converter that provides energy management among the dc buses, and ac-dc charging functionalities. Its main advantage with respect to linear techniques is that the control design includes the inherent nonlinearities of the model. Indeed, an appropriate control and state variables transformation is proposed that linearizes and decouples the system, and a PI controller rendering asymptotic stability and robustness to resistive load changes and presence of CPLs is devised. Then, the control transformation, which involves nonlinear terms, is inverted using linear approximations, and no major performance decay is observed. This paper combines the modelling approach presented in [24] with the feedback linearizating controller proposed in [37]. The main contribution is related to the experimental validation of the nonlinear control approach.

The remainder of the paper is organized as follows. The behavioural model of the multiport dc-dc converter is presented in Section II. The feedback linearizing control strategy and some issues related to the inversion of the control law are discussed in Section III. The description of the experimental setup and some experimental results are discussed in Section IV and, finally, conclusions and some suggestions for further research are drawn in Section V.

II. BEHAVIOURAL MODEL OF THE CONVERTER

Fig. 2 shows the schematic of the magnetically coupled multiport dc-dc converter. It consists of a n-port high frequency transformer with N_k, $k \in \{1, 2, \ldots, n\}$, turns at each of its windings, and a full-bridge converter connected to each of the transformer ports. The converters have a capacitor C_k in their dc side.

To establish a model of the multiport converter based on the power flow between the transformer ports, the following assumptions are considered:

A1 The magnetising inductances and the parasitic conduction losses are not considered.

A2 The power transfer dynamics in the transformer is several orders of magnitude faster than the dynamics of the full converter (fixed by the values of the dc bus capacitors of the full-bridge converters). Thus, the power transfer in the high frequency transformer can be considered instantaneous and it can be modelled algebraically.

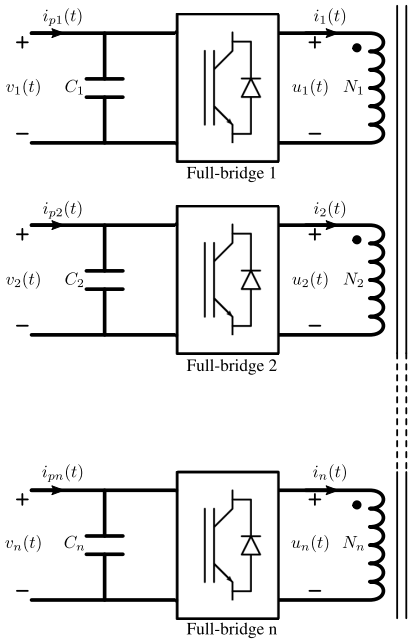

FIGURE 2. Multiport dc-dc converter.

A3 The modulation signals, $\beta_k(t)$, are zero-average periodic bipolar square wave signals with fundamental frequency ω_1 and phase shift θ_k, i.e. $\beta_k(t) = \text{sign}(\sin(\omega_1 t - \theta_k))$ $k \in \{1, 2, \ldots, n\}$.

Under Assumptions A1 and A2, the dc bus voltages of the full-bridge converters can be assumed constant, i.e. $v_k(t) = V_k$, $k \in \{1, 2, \ldots, n\}$, and the full-bridge converter operation generates periodic bipolar symmetric square-wave voltages[1] of constant amplitude, duty ratio equal to 0.5 and phase shift θ_k. That is,

$$u_k(t) = V_k \beta_k(t) = V_k \,\text{sign}(\sin(\omega_1 t - \theta_k)), \tag{1}$$

where $\omega_1 = \frac{2\pi}{T}$ is the fundamental frequency of the periodic voltages and currents in the transformer, and T the fundamental period of the signal.

Notice that the voltages $u_k(t)$ at the transformer windings are square signals with zero mean and the control variables of the converter are, then, the relative phases between the voltages. The currents at the windings $i_k(t)$ have also zero mean because the transformer is considered to be a linear system and the power transfer analysis is carried out in the steady state. It is worth remarking that the power transfer in the transformer is done at the fundamental frequency of the voltage signals and their harmonics.

A. POWER FLOW ANALYSIS AT A GIVEN PORT k

Fig. 3 represents the electrical equivalent circuit referred to any port k, when applying the port voltages (1) and, under Assumption A1, the magnetising inductances are disregarded. In figure 3, L_{dk} refers to leakage inductance at port

[1]These signals verify $u_k(t) = -u_k(t + \frac{T}{2})$, $\forall t$. This property is equivalent to have, in their Fourier series developments, null harmonic content in the even harmonics including the zero one.

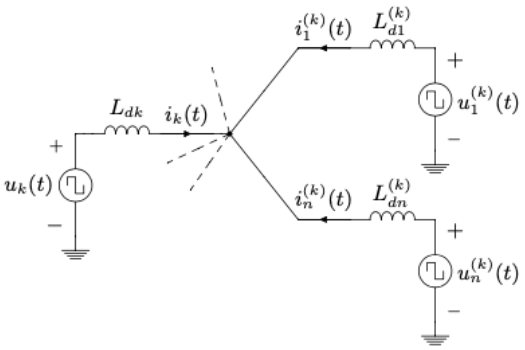

FIGURE 3. Electrical equivalent circuit for the multiport dc-dc converter, where the magnetising inductances are neglected.

k, and $L_{d1}^{(k)}, \ldots, L_{dn}^{(k)}$ refer to the reflected leakages at port k from ports 1 to n (except k). See further details in [24]. Under periodic regime, the Fourier series development of the voltage at port k, and the voltage at port $l \neq k$ referred to port k are

$$u_k(t) = \sum_{h=-\infty}^{\infty} c_{k,h} e^{jh\omega_1 t}, \tag{2}$$

$$u_l^{(k)}(t) = \sum_{h=-\infty}^{\infty} c_{l,h}^{(k)} e^{jh\omega_1 t}, \tag{3}$$

respectively, where $h \in \mathbb{Z}$, and

$$c_{k,h} = \begin{cases} -j\dfrac{2\,V_k}{h\pi} e^{-jh\theta_k}, & h \mod 2 \neq 0 \\ 0, & h \mod 2 = 0 \end{cases} \tag{4}$$

$$c_{l,h}^{(k)} = \begin{cases} -j\dfrac{2(V_l/\alpha_{kl})}{h\pi} e^{-jh\theta_l}, & h \mod 2 \neq 0 \\ 0, & h \mod 2 = 0 \end{cases} \tag{5}$$

where $\alpha_{kl} = \frac{N_l}{N_k}$, $k, l \in \{1, 2, \ldots, n\}$, $k \neq l$, is the transformer turn ratio of the k-th port with respect to the l-th port and $h \in \mathbb{Z}$.

Using Rosen's Theorem [38], the nodal network in Fig. 3 is transformed into a meshed one where the linking inductance between port k and any l-th port is given by

$$L_{kl}^{(k)} = L_{dk} L_{dl}^{(k)} \sum_{m=1}^{n} \frac{1}{L_{dm}^{(k)}}, \tag{6}$$

and the (virtual) current flowing between ports k and l is

$$i_{kl}(t) = \sum_{h=-\infty}^{\infty} d_{kl,h} e^{jh\omega_1 t} \tag{7}$$

where

$$d_{kl,h} = \frac{c_{k,h} - c_{l,h}^{(k)}}{jh\omega_1 L_{kl}^{(k)}}. \tag{8}$$

The total averaged (active) power injected from port k is

$$P_k = \sum_{l=1, l\neq k}^{n} P_{kl}, \tag{9}$$

where[2]

$$P_{kl} = \frac{1}{T}\int_{t-T}^{t} u_k(\tau)\,\overline{i_{kl}}(\tau)\,d\tau. \tag{10}$$

Using (2) and (7)

$$P_{kl} = c_{k,0}d_{kl,0} + 2\,\mathrm{Re}\left\{\sum_{h=1}^{\infty} c_{k,h}\,\overline{d_{kl,h}}\right\} \tag{11}$$

that can be written as

$$P_{kl} = -\frac{j2\,V_k V_l}{\alpha_{kl}\pi^2\omega_1\,L_{kl}^{(k)}}\Big(\mathrm{Li}_3(e^{j\delta_{kl}}) - \mathrm{Li}_3(-e^{j\delta_{kl}}) - \mathrm{Li}_3(e^{-j\delta_{kl}}) + \mathrm{Li}_3(-e^{-j\delta_{kl}})\Big) \tag{12}$$

where $\delta_{kl} = \theta_l - \theta_k$ and $\mathrm{Li}_a(z) = \sum_{r=1}^{\infty}\frac{z^r}{r^a}$ is the polylogarithm function. Fig. 4 shows graphically, in red, the relation[3] among P_{kl} and δ_{kl} for $\delta_{kl} \in [-\pi, \pi]$, which is equivalent to a temporal delay $[-\frac{T}{2}, \frac{T}{2}]$ between the voltages at the ports.

Expanding the transferred power P_{kl} in series around $\delta_{kl} = 0$ results in

$$P_{kl} = \frac{V_k V_l}{\alpha_{kl}\omega_1\,L_{kl}^{(k)}}\left(\delta_{kl} - \frac{\mathrm{sign}(\delta_{kl})\delta_{kl}^2}{\pi}\right) + O(\delta_{kl}^M). \tag{13}$$

It is worth remarking that the order M can be anyone, and that the agreement between

$$P_{kl}^{\text{approx}} = \frac{V_k V_l}{\alpha_{kl}\omega_1\,L_{kl}^{(k)}}\left(\delta_{kl} - \frac{\mathrm{sign}(\delta_{kl})\delta_{kl}^2}{\pi}\right) = \frac{V_k V_l}{\alpha_{kl}\omega_1 L_{kl}^{(k)}}\,\delta_{kl}\left(1 - \frac{|\delta_{kl}|}{\pi}\right) \tag{14}$$

and P_{kl} in (12) is perfect in the interval $\delta_{kl} \in [-\pi, \pi]$, see Fig. 4. Equation (14) is the usually stated in the previous literature, e.g. [39]. Finally, the total power transferred to port k results in

$$P_k = \frac{V_k}{\omega_1}\sum_{l=1, l\neq k}^{n}\frac{V_l}{\alpha_{kl}L_{kl}^{(k)}}\,\delta_{kl}\left(1 - \frac{|\delta_{kl}|}{\pi}\right). \tag{15}$$

B. MULTIPORT DC-DC CONVERTER

Using the total power transferred at port k of (15), the voltage dynamics at each port is given by the Kirchhoff Current Law and the capacitor dynamics giving

$$C_k\dot{v}_k = i_{pk} - \frac{1}{v_k}P_k. \tag{16}$$

Therefore, the voltage dynamics at each port of the multiport converter is described by the nonlinear ordinary differential equations system

$$C_k\dot{v}_k = i_{pk} - \frac{1}{\omega_1}\sum_{l=1, l\neq k}^{n}\frac{v_l}{\alpha_{kl}L_{kl}^{(k)}}\,\delta_{kl}\left(1 - \frac{|\delta_{kl}|}{\pi}\right), \tag{17}$$

where $k, l \in \{1, 2, \ldots, n\}$.

[2] $\bar{a}$ means the conjugate of the complex number a.

[3] It is worth noting that $P_{kl}(\delta_{kl})$ is 2π-periodic in δ_{kl}.

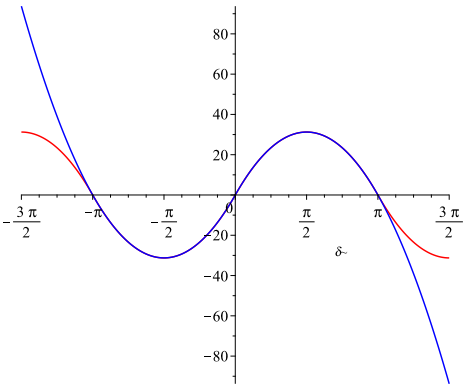

FIGURE 4. Power transferred from ports l to k, P_{kl} (W), with respect to δ_{kl} (rad). Exact relationship, eq. (12), in red, and approximation, eq. (14), in blue. The used parameters are $V_k = 100$ V, $V_l = 100$ V, $\omega_1 = 2\pi\,40.0 \cdot 10^3$ rad/s, $L_{kl} = 1.0$ mH and $\alpha_{kl} = 1$.

In the following sections the particular case of a 3-port converter is used assuming that port number 1 is fed at constant voltage E_1.

Besides, the load currents at ports 2 and 3 are assumed as composed by a resistive component and a constant power component, i.e. $i_{pk} = -\left(\frac{v_k}{R_k} + \frac{P_k}{v_k}\right)$. This assumption allows to consider the possible connection to the dc ports of the multiport converter of resistive and converter-interfaced dc loads.

III. CONTROLLER DESIGN

As mentioned at the end of last Section, let us to consider a three dc bus system: a high voltage dc bus (nominal voltage 400 V) and two low voltage buses (nominal voltages 48 V and 12 V). The voltage at the 365 V bus is assumed constant (mainly, due to the usual high capacity battery in these buses) and the two other buses have several loads connected to them. Setting the phase shift for port 1 as the reference, i.e., $\theta_1 = 0$, the system dynamics is given by:

$$C_2\dot{v}_2 = -\frac{v_2}{R_2} - \frac{P_2}{v_2} + \frac{E_1}{\omega_1\alpha_{12}L'_{12}}\theta_2\left(1 - \frac{|\theta_2|}{\pi}\right) + -v_3\frac{1}{\omega_1\alpha_{23}L'_{23}}(\theta_3 - \theta_2)\left(1 - \frac{|\theta_3 - \theta_2|}{\pi}\right) \tag{18a}$$

$$C_3\dot{v}_3 = -\frac{v_3}{R_3} - \frac{P_3}{v_3} + \frac{E_1}{\omega_1\alpha_{13}L'_{13}}\theta_3\left(1 - \frac{|\theta_3|}{\pi}\right) + v_2\frac{1}{\omega_1\alpha_{32}L'_{32}}(\theta_3 - \theta_2)\left(1 - \frac{|\theta_3 - \theta_2|}{\pi}\right), \tag{18b}$$

where v_2 is the voltage of the 48 V bus, v_3 is the voltage of the 12 V bus, and the phase shifts in ports 2 and 3, namely θ_2, θ_3, respectively, are the control variables, with $\theta_i \in \left[-\frac{\pi}{2}, \frac{\pi}{2}\right]$, $i \in \{2, 3\}$.

The control objectives are to regulate the voltages v_2 and v_3 to the reference values, $v_2^* = 48$ V and $v_3^* = 12$ V, in spite of the load variations in the buses (described by R_i, P_i, respectively). For control design purposes it is assumed that the voltages at the buses are available for measure.

Let

$$f_i(\theta_i) = \frac{E_1}{\omega_1 \alpha_{1i} L'_{1i}} \theta_i \left(1 - \frac{|\theta_i|}{\pi}\right), \quad i = 2, 3$$
$$\lambda_i = \frac{1}{\omega_1 \alpha_{ij} L'_{ij}}, \quad i = 2, 3, \quad i \neq j,$$
$$g(\theta_2, \theta_3) = (\theta_3 - \theta_2)\left(1 - \frac{|\theta_3 - \theta_2|}{\pi}\right).$$

Then, (18) becomes

$$C_2 \dot{v}_2 = -\frac{v_2}{R_2} - \frac{P_2}{v_2} + f_2(\theta_2) - \lambda_2 v_3 g(\theta_2, \theta_3) \quad (19a)$$
$$C_3 \dot{v}_3 = -\frac{v_3}{R_3} - \frac{P_3}{v_3} + f_3(\theta_3) + \lambda_3 v_2 g(\theta_2, \theta_3). \quad (19b)$$

The selected control law uses a feedback linearization approach. Let us consider the change of state variables

$$\xi_i = v_i^2, \quad (20)$$

with the subindex i taking the values $i = 2, 3$ unless otherwise stated below, and the change of control variables

$$u_2 = v_2 f_2(\theta_2) - \lambda_2 v_2 v_3 g(\theta_2, \theta_3) \quad (21a)$$
$$u_3 = v_3 f_3(\theta_3) + \lambda_3 v_2 v_3 g(\theta_2, \theta_3). \quad (21b)$$

Then, (19) boils down to the linear, decoupled system

$$\dot{\xi}_i = -\frac{2}{R_i C_i}\xi_i - \frac{2P_i}{C_i} + \frac{2}{C_i} u_i. \quad (22)$$

Let ξ_i^* denote the reference for the state variable ξ_i. Then, consider the following PI controller,

$$u_i = -k_{pi}\xi_i + k_{zi} z_i \quad (23a)$$
$$\dot{z}_i = \xi_i^* - \xi_i, \quad (23b)$$

with k_{pi}, k_{zi} verifying:

$$\frac{1}{R_i} + k_{pi} > 0, \quad k_{zi} > 0. \quad (24)$$

Proposition 1: The closed-loop system (22), (23), (24) *shows a unique equilibrium point* $\left(\xi_2^*, z_2^*, \xi_3^*, z_3^*\right)^\top$, *with*

$$z_i^* = \frac{1}{k_{zi}}\left[\left(\frac{1}{R_i} + k_{pi}\right)\xi_i^* + P_i\right], \quad (25)$$

which is globally asymptotically stable.

Proof: The closed-loop system (22), (23) is given by

$$\dot{\xi}_i = -\frac{2}{C_i}\left(\frac{1}{R_i} + k_{pi}\right)\xi_i - \frac{2P_i}{C_i} + \frac{2k_{zi}}{C_i} z_i, \quad (26a)$$
$$\dot{z}_i = \xi_i^* - \xi_i, \quad (26b)$$

and it is immediate to check that it shows a single equilibrium at $\left(\xi_2^*, z_2^*, \xi_3^*, z_3^*\right)^\top$, with z_i^* verifying (25). Now, defining $e_i = \xi_i - \xi_i^*$, $e_{zi} = z_i - z_i^*$, (26) becomes linear:

$$\dot{e}_i = -\frac{2}{C_i}\left(\frac{1}{R_i} + k_{pi}\right) e_i + \frac{2k_{zi}}{C_i} e_{zi} \quad (27)$$

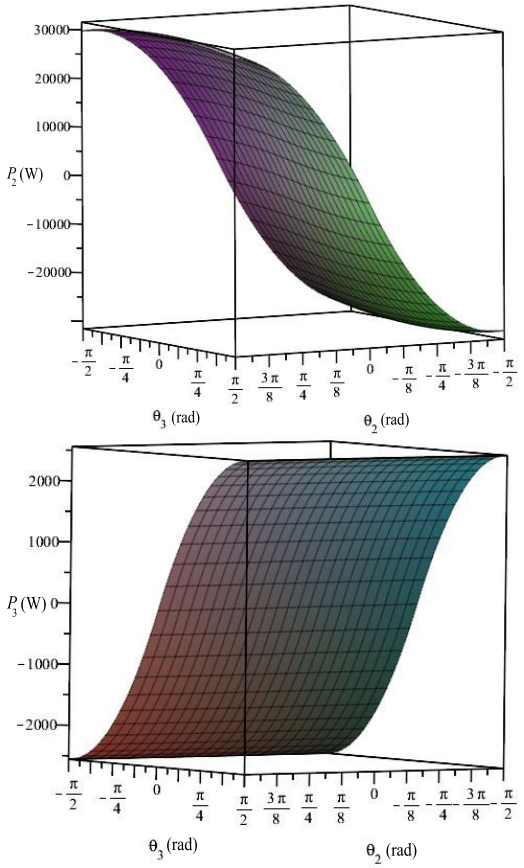

FIGURE 5. Top: $u_2 = u_2(\theta_2, \theta_3)$; bottom: $u_3 = u_3(\theta_2, \theta_3)$.

$$\dot{e}_{zi} = -e_i. \quad (28)$$

Finally, it follows straightforward that its characteristic polynomial is

$$p(\chi) = \prod_{i=2}^{3}\left[\chi^2 + \frac{2}{C_i}\left(\frac{1}{R_i} + k_{pi}\right)\chi + \frac{2k_{zi}}{C_i}\right],$$

which has all its roots in the left complex plane if and only if (24) is fulfilled. Then, the result follows. □

Remark: It stems immediately from the previous result that $k_{pi}, k_{zi} > 0$ is sufficient to ensure that the control law (23) guarantees robustness to parametric uncertainty on R_i, P_i. The main issue with this control law is in the inversion of the change of variables (21), which is analyzed below.

The control law (21) is highly nonlinear, as it involves absolute value terms. In order to carry out the inversion, i.e. to obtain $\theta_i = \theta_i(u_2, u_3)$, we may first notice from Figure 5 that the $\mathbb{R}^3$ surfaces defined in (21) have a large range within its domain, $\theta_i \in \left[-\frac{\pi}{2}, \frac{\pi}{2}\right]$. However, taking into account that u_i has power units, and that the range of admissible power is, approximately, $u_2 \in [0, 2400W]$, $u_3 \in [0, 600W]$, the zoom in Figure 6 discloses a linear behavior of the surfaces in such region.

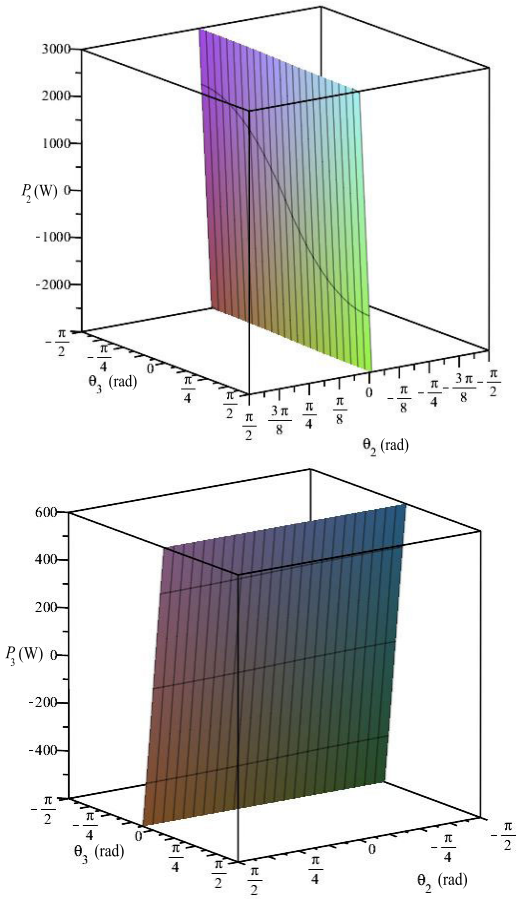

FIGURE 6. Zoom of Figure 5. Top: $u_2 = u_2(\theta_2, \theta_3)$; bottom: $u_3 = u_3(\theta_2, \theta_3)$.

This is consistent with the fact that, although

$$\theta\left(1 - \frac{|\theta|}{\pi}\right)$$

is nicely approximated by $\frac{\pi}{4}\sin\theta$ in $\left[-\frac{\pi}{2}, \frac{\pi}{2}\right]$, the identity, θ, does better in a neighbourhood of $\theta = 0$, as plotted in Figure 7. Hence, the inversion will be performed from the linear approximation of the change of variables (21), namely,

$$u_2 \approx v_2\left(k_2\theta_2 - \lambda_2 v_3\left(\theta_3 - \theta_2\right)\right) \tag{29a}$$

$$u_3 \approx v_3\left(k_3\theta_3 + \lambda_3 v_2\left(\theta_3 - \theta_2\right)\right), \tag{29b}$$

with

$$k_i = \frac{E_1}{\omega_1 \alpha_{1i} L'_{1i}}.$$

Therefore:

$$\theta_2 \approx \frac{\left(\lambda_3 + \frac{k_3}{v_2}\right)u_2 + \lambda_2 u_3}{\lambda_3 k_2 v_2 + \lambda_2 k_3 v_3 + k_2 k_3} \tag{30a}$$

$$\theta_3 \approx \frac{\lambda_3 u_2 + \left(\lambda_2 + \frac{k_2}{v_3}\right)u_3}{\lambda_3 k_2 v_2 + \lambda_2 k_3 v_3 + k_2 k_3}, \tag{30b}$$

where the control actions u_i are defined in (23).

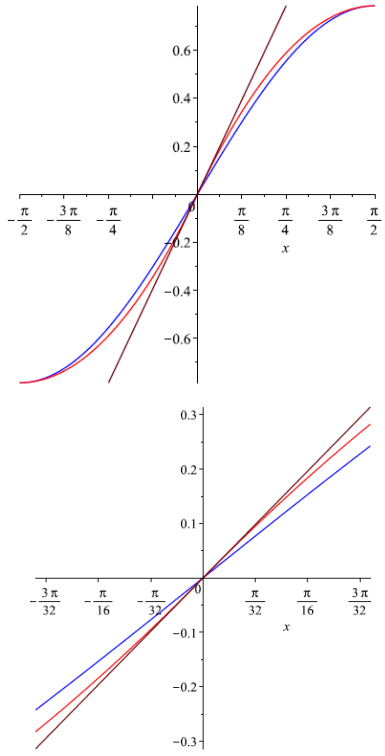

FIGURE 7. Red: $\theta\left(1 - \frac{|\theta|}{\pi}\right)$; blue: $\frac{\pi}{4}\sin\theta$; brown: θ. Top: $\theta \in \left[-\frac{\pi}{2}, \frac{\pi}{2}\right]$; bottom: $\theta \in \left[-\frac{3\pi}{32}, \frac{3\pi}{32}\right]$.

TABLE 1. Experimental multiport DC/DC converter details.

Parameter	Symbol	Value
Port number	-	3 (1 battery port, 2 ports regulated)
Battery voltage	v_1	365 V
Reference voltages Bus 2, 3	v_2^* v_3^*	48 / 12 V
Nominal currents Bus 2, 3	i_{p2} i_{p3}	50 / 12 A
Output capacitance Bus 2, 3	C_2, C_3	200 / 600 μC
Transformer windings turns	N_1 / N_2 / N_3	24 / 3 / 0.8
Transformer magnetizing inductance	L_m	2 mH
Transformer leakage inductances	$L_{12}^{(2)}, L_{13}^{(3)}$	0.4 μH, 1 μH
Auxiliar leakage inductances	$L_{12_a}^{(2)}, L_{13_a}^{(3)}$	2.6 μH, 1.5 μH
Switching frequency	f_{sw}	40 kHz
Controller gains		
48 V (v_2) bus controller	k_{p2}, k_{z2}	$8 \cdot 10^3$, $24 \cdot 10^6$
12 V (v_3) bus controller	k_{p3}, k_{z3}	$15 \cdot 10^4$, $240 \cdot 10^6$

The equivalent block diagram of the proposed controller is shown in Figure 8, where the specific equations of each functional block have been detailed.

IV. EXPERIMENTAL SETUP AND RESULTS

For the experimental evaluation of the proposed converter with the designed controller, a 2.5 kW experimental prototype has been built. The main parameters of the power stage are detailed in Table 1.

A. DESCRIPTION OF THE PLANT

The experimental prototype is shown in Figures 9, 10. The converter has been developed in a single board where the

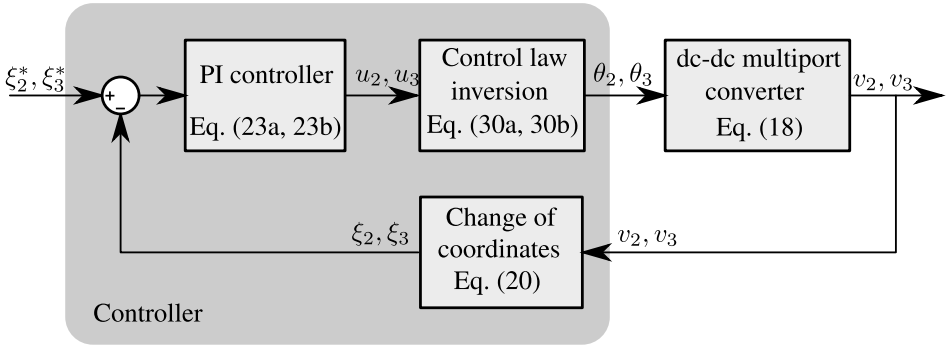

FIGURE 8. Block diagram of the proposed controller.

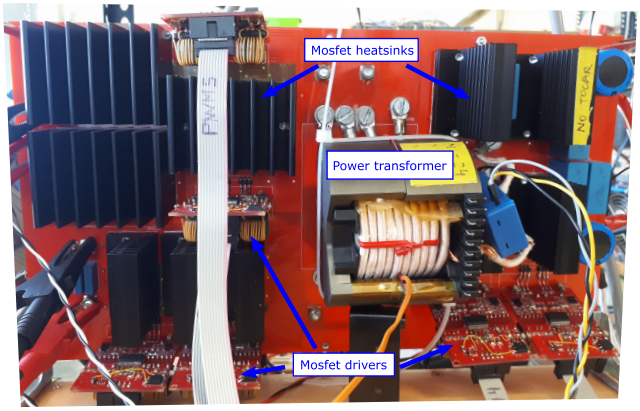

FIGURE 9. Experimental prototype. Front view highlighting the power transformer, the MOSFETs heat sinks and drivers.

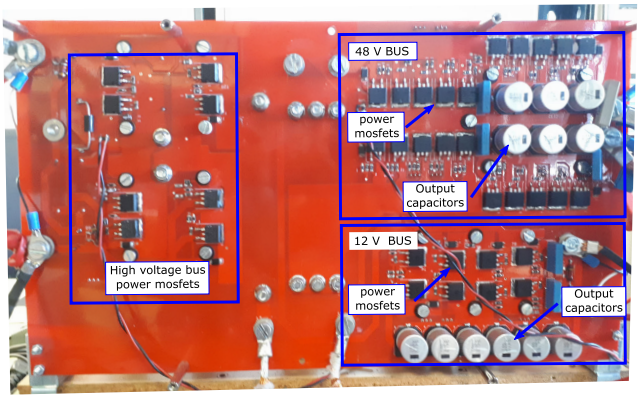

FIGURE 10. Experimental prototype. back view highlighting the power MOSFETs and output capacitors.

power MOSFETs, the heat sinks and the power transformer have been assembled in a compact form. The power devices have been placed in one side of the board and the heat sinks at the other, minimizing the thermal path for the losses dissipation without active cooling. According to the nominal power of the buses, the MOSFETs have been grouped in parallel in order to manage the current of the converter with low losses. Specifically, two STB45N65M5 have been used in the primary side, five IRFS4310 have been used in the 48 V bus and two IPB120N04S4 for the 12 V bus. The gate drivers used for the power switches are based on the Infineon 2ED020I12FA chip, which provides isolated driving, protecting the control stage from undesirable noises of the power stage. In the experimental part, the high voltage bus has been set to 365 V instead of 400 to facilitate the transformer construction, which has been wound by hand. The power transformer has been assembled using a P87/70-N87 ferrite core, wounded with copper litz wire, thus minimizing the high frequency losses produced by the skin effect. In order to ensure a low core flux without saturation, 24 turns have been used for the high voltage side, 3 turns for the 48 V bus and 0.8 turns for the 12 V one.[4] The effective leakage inductances of the transformer have been increased by two auxiliary inductors placed in series at the secondary sides, adapting the system gain to the power level (See Table 1). Finally, the voltage sensing is implemented by voltage dividers through isolation barriers (HCPL-790B). In the acquisition chains to the ADCs (Analogue to Digital Converters), first order low pass filters with a cut off frequency of 10 kHz have been used. The transformer currents are measured for monitoring and fault detection purpose, not being required by the controllers.

The equipment used in the experimental evaluation were the voltage a TDK-Lambda GEN 600-17 voltage source, a Chroma 63804 AC/DC electronic load, several Fluke True RMS 175 multimeters and a Yogokawa DLM 2024 oscilloscope with 700924 voltage probes and 701931 current probes.

The controllers have been digitally implemented using a Texas Instruments F28379D DSP microcontroller. The code has been programmed using only one of the cores available in that device. The sampling frequency of the control routine is 40 kHz which is the same as the fundamental frequency of the square bipolar voltages in the converter full-bridges.

B. EXPERIMENTAL RESULTS

In the experimental results the converter has been assessed in terms of steady-state performance, evaluating the load and line regulations and the converter's efficiency, and also in

[4]To obtain a fractional ratio, the turn was not completely closed [40] and the effective turn ratio was empirically confirmed.

TABLE 2. Line regulation of the experimental prototype.

No load			Mid Load 48V@16A, 12V@6A			Full Load 48V@42 A, 12V@12A		
v_1 (V)	v_2 (V)	v_3 (V)	v_1 (V)	v_2 (V)	v_3 (V)	v_1 (V)	v_2 (V)	v_3 (V)
330	12.13	47.91	330	12.07	47.93	330	12.07	47.92
365	12.08	47.94	365	12.08	47.92	365	12.08	47.92
400	12.08	47.95	400	12.08	47.91	400	12.08	47.92

TABLE 3. Load regulation of the experimental prototype.

12 V Bus					
Output Power (W)	0	36	72	108	144
Output Voltage (V)	12.08	12.08	12.07	12.07	12.07
48 V Bus					
Output Power (kW)	0	0.5	1	1.5	2
Output Voltage (V)	47.93	47.92	47.93	47.94	47.92

TABLE 4. Converter efficiency.

Total output Power (kW)	0	0.15	0.84	2	2.4
Efficiency (%)	-	83.1	91.4	95.5	95.2
Losses (W)	23	30	79	94	121

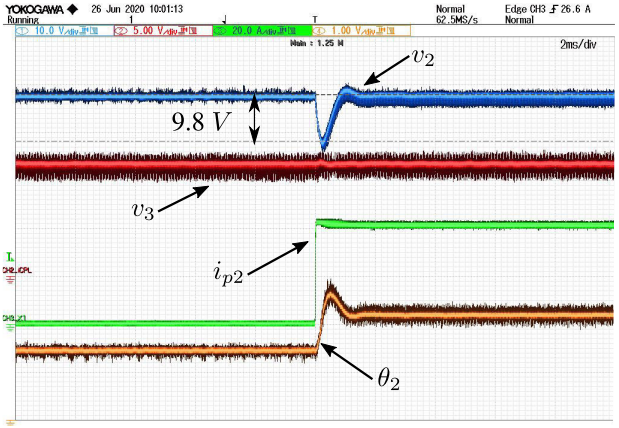

FIGURE 11. Transient under a 2 kW CPL connection at the 48 V bus, 12 V bus without load. v_2 (blue, 10 V/div), v_3 (red, 5 V/div), i_{p2} (green, 20 A/div), θ_2 (orange, 60 °/div).

terms of transient response, testing both resistive and constant power loads.

1) STEADY-STATE EXPERIMENTAL RESULTS

The line and load regulation, and the converter efficiency of the converter, are shown in Tables 2, 3 and 4, respectively. The results confirm the good behaviour of the converter with the designed controller. The converter has been evaluated in a range of ±10 % of the nominal input voltage, guaranteeing

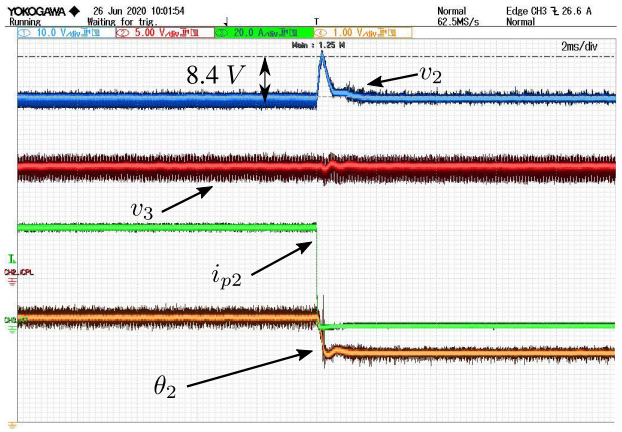

FIGURE 12. Transient under a 2 kW CPL disconnection at the 48 V bus, 12 V bus without load. v_2 (blue, 10 V/div), v_3 (red, 5 V/div), i_{p2} (green, 20 A/div), θ_2 (orange, 60 °/div).

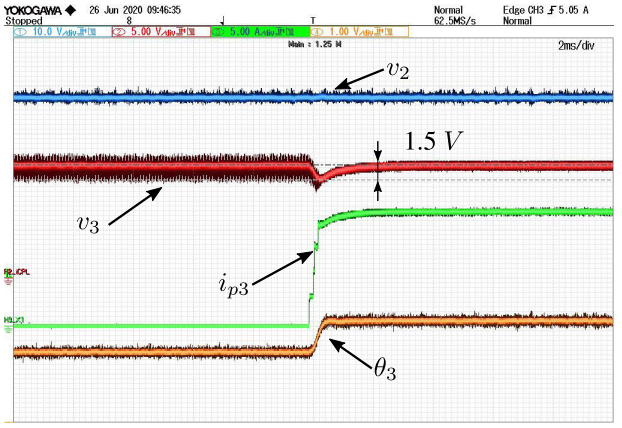

FIGURE 13. Transient under a resistive load connection at the 12 V bus, 48 V bus without load. v_2 (blue, 10 V/div), v_3 (red, 5 V/div), i_{p3} (green, 5 A/div), θ_3 (orange, 60 °/div).

regulated voltages at their outputs in that range with a very small deviation from the nominal values. Similarly, the output currents do not reduce the output voltage regulation, as Table 3 reveals, since the output voltages slightly vary as the output power increases. The converter efficiency was measured in the working points shown in Table 4. The measured values are adequate for a first experimental prototype.

2) TRANSIENT RESPONSE EXPERIMENTAL RESULTS

In order to evaluate the transient response of the converter in front of load variations different tests have been performed. The first test consists in applying a CPL transient in the 48 V bus from no load to 2 kW and from 2 kW to no load, while the 12 V bus is maintained in no load condition. The Figures 11 and 12 show the load transients due to the 2 kW CPL. The signals shown in the oscilloscope captures are: 48 V bus voltage, v_2, in channel 1 (blue), 12 V bus voltage, v_3, in channel 2 (red), 48 V bus load current, i_{p2}, in channel 3 (green) and 48 V bus control action, θ_2, in channel 4 (orange). The control action is plotted using a digital-to-analog converter (DAC) of the micro controller, where 3 V corresponds

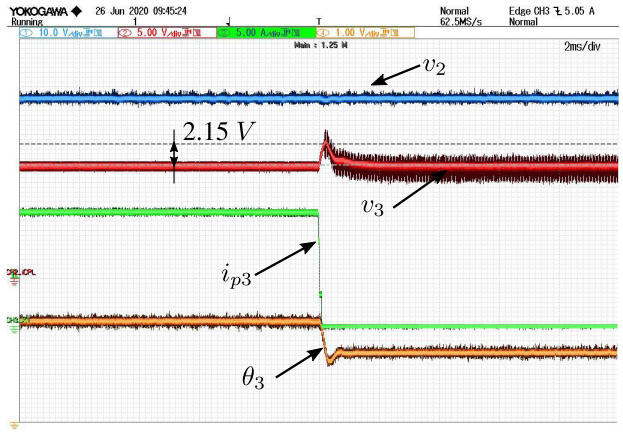

FIGURE 14. Transient under a resistive load disconnection at the 12 V bus, 48 V bus without load. v_2 (blue, 10 V/div), v_3 (red, 5 V/div), i_{p3} (green, 5 A/div), θ_3 (orange, 60 °/div).

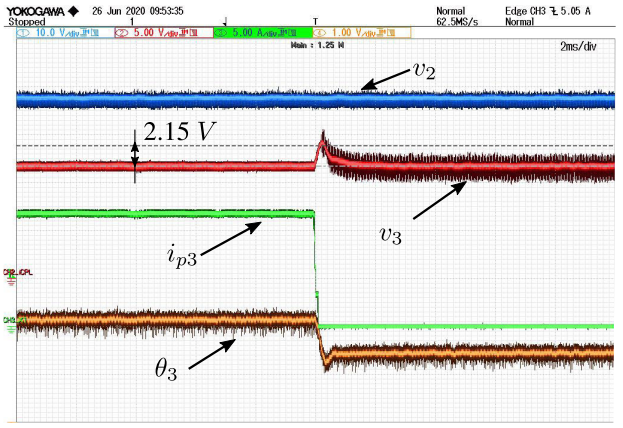

FIGURE 16. Transient under a resistive load disconnection at the 12 V bus, 48 V bus with 2 kW CPL. v_2 (blue, 10 V/div), v_3 (red, 5 V/div), i_{p3} (green, 5 A/div), θ_3 (orange, 60 °/div).

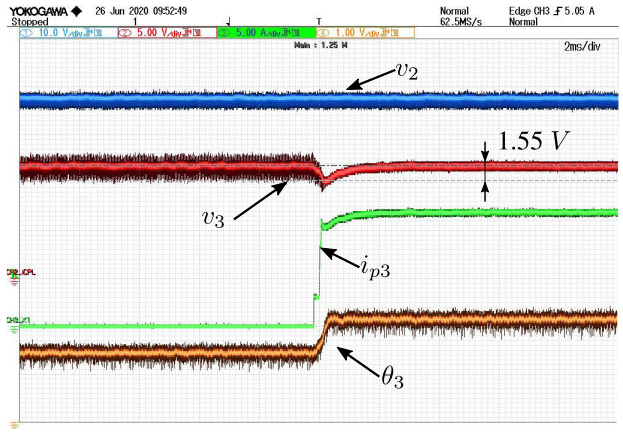

FIGURE 15. Transient under a resistive load connection at the 12 V bus, 48 V bus with 2 kW CPL. v_2 (blue, 10 V/div), v_3 (red, 5 V/div), i_{p3} (green, 5 A/div), θ_3 (orange, 60 °/div).

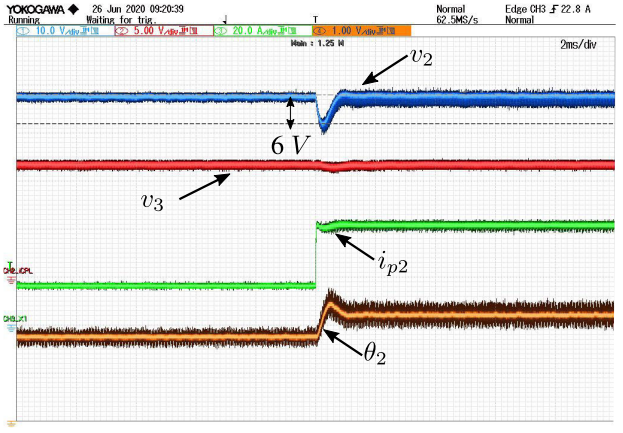

FIGURE 17. Transient under a 1.25 kW CPL connection at the 48 V bus with 3 Ω load, 12 V bus with 1 Ω load. v_2 (blue, 10 V/div), v_3 (red, 5 V/div), i_{p2} (green, 20 A/div), θ_2 (orange, 60 °/div).

to 90° and 0 V to -90°. From the results, the good behaviour of the controller in front of CPL transients can be inferred, being the maximum error during the transient of 9.8 V representing the 20% of its nominal voltage and recovering the regulated value in 1 ms with a smooth transient. In both results, it can be seen how the transients in 48 V bus do not affect the 12 V bus, thus confirming the decoupled performance of the converter outputs. Notice from the current shape (green signal) the CPL load behaviour.

The transient response of the 12 V bus is evaluated in the next test. Figures 13 and 14 depict resistive load transients when a resistor of 1 Ω is connected and disconnected while the 48 V bus voltage is in no load condition. In this case, the signals shown in the oscilloscope captures are: 48 V bus voltage, v_2, in channel 1 (blue), 12 V bus voltage, v_3, in channel 2 (red), 12 V bus load current, i_{p3}, in channel 3 (green) and 48 V bus control action, θ_3, in channel 4 (orange). The control action is plotted again using a DAC of the micro controller with the same scale as before. Now, the maximum voltage deviation at bus 3 is around 2 V in both transients, which represent a 16% of the desired value, recovering the nominal value in 2 ms. Again, the voltage at bus 2 is not affected by bus 3 transients. The current profile in Figure 13 allows to identify the resistive behaviour of the load used in this test.

The same tests shown in Figures 13 and 14 are repeated with the main bus loaded with a 2 kW CPL, and their results are shown in Figures 15 and 16. The transient results are similar under the two load conditions, and the dynamic decoupling of the controllers is confirmed.

Finally, an experimental test combining resistive and CPL loads is presented. Figures 17 and 18 show a CPL transient of 1.25 kW at the 48 V bus while it is simultaneously loaded with 3 Ω (16 A) and the 12 V bus is loaded with 1 Ω (12 A). The signals shown in oscilloscope captures are: 48 V bus voltage, v_2, in channel 1 (blue), 12 V bus voltage, v_3, in channel 2 (red), 48 V bus load current, i_{p2}, in channel 3 (green) and 48 V bus control action, θ_2, in channel 4 (orange). The control action is plotted, as previously, using a DAC of the micro controller.

The results corroborate again the good behaviour of the controller while manage both type of loads, resistive and

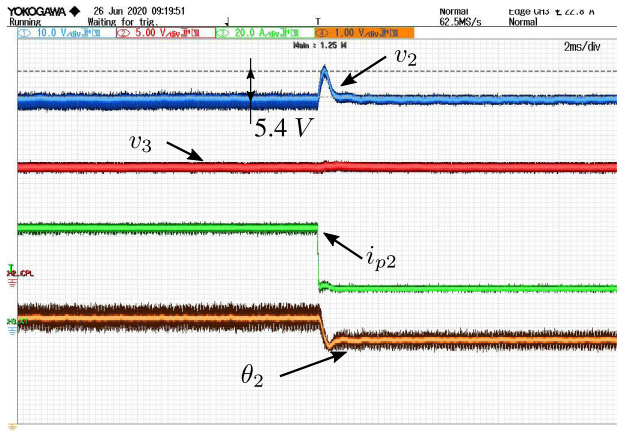

FIGURE 18. Transient under a 1.25 kW CPL disconnection at the 48 V bus with 3 Ω load, 12 V bus with 1 Ω load. v_2 (blue, 10 V/div), v_3 (red, 5 V/div), i_{p2} (green, 20 A/div), θ_2 (orange, 60 °/div).

CPL. The voltage of the 48 V bus suffers a maximum variation of 6 V, recovering the nominal value, which represents an error of 12 %, and the steady-state value is recovered in around 1 ms. Notice how, again, the voltage at bus 3 is almost unaffected, thus confirming that the decoupled behaviour of the controllers does not depend neither on the operation point nor on the load nature (resistive or CPL).

V. CONCLUSION

This article has shown a detailed obtaining of a dynamic model, based on the average power flow among the ports, for a magnetically-coupled multiport dc-dc converter. Using this model, a feedback linearization-based controller has been designed. The controller, through an appropriate change of control and state variables, linearizes and decouples the model thus allowing to design a simple, yet efficient, outer conventional PI controller. The inversion of the nonlinear control transformation has been carried out using linear approximations without observing a significant loss of performance.

In order to validate the proposed control law, a three-port experimental prototype has been built. The experiments that have been carried out with it show the good operation of the controlled system in front of different operational situations.

Further research is currently oriented to the development of new adaptive and robust control laws for the multiport converter.

REFERENCES

[1] Use of New Energies in Road Transport, "European green vehicles initiative PPP," Rep. Eur. Commission, Horizon City, TX, USA, 2020.
[2] G. Meyer, J. Dokic, H. Jürgens, and D. M. Tobias, "Hybrid and electric vehicles—The electric drive commutes," Int. Energy Agency, Tech. Rep., 2016.
[3] C. C. Chan, "The state of the art of electric, hybrid, and fuel cell vehicles," *Proc. IEEE*, vol. 95, no. 4, pp. 704–718, Apr. 2007.
[4] O. Coppin, "From 12+12V to 48V: A new road map for hybridization," in *Proc. Engine Expo*, 2016.
[5] B. Farhangi and H. A. Toliyat, "Modeling and analyzing multiport isolation transformer capacitive components for onboard vehicular power conditioners," *IEEE Trans. Ind. Electron.*, vol. 62, no. 5, pp. 3134–3142, May 2015.
[6] C. Gu, Z. Zheng, L. Xu, K. Wang, and Y. Li, "Modeling and control of a multiport power electronic transformer (PET) for electric traction applications," *IEEE Trans. Power Electron.*, vol. 31, no. 2, pp. 915–927, Feb. 2016.
[7] B. Karanayil, M. Ciobotaru, and V. G. Agelidis, "Power flow management of isolated multiport converter for more electric aircraft," *IEEE Trans. Power Electron.*, vol. 32, no. 7, pp. 5850–5861, Jul. 2017.
[8] C. Gu, H. Yan, J. Yang, G. Sala, D. De Gaetano, X. Wang, A. Galassini, M. Degano, X. Zhang, and G. Buticchi, "A multiport power conversion system for the more electric aircraft," *IEEE Trans. Transport. Electrific.*, vol. 6, no. 4, pp. 1707–1720, Dec. 2020.
[9] Z. Qian, "Modeling and design of multi-port DC/DC converters," Ph.D. dissertation, Dept. Elect. Eng. Comput. Sci., Univ. Central Florida, Orlando, FL, USA, 2010.
[10] H. Tao, J. L. Duarte, and M. A. M. Hendrix, "Three-port triple-half-bridge bidirectional converter with zero-voltage switching," *IEEE Trans. Power Electron.*, vol. 23, no. 2, pp. 782–792, Mar. 2008.
[11] T. Chaudhury and D. Kastha, "A high gain multiport DC–DC converter for integrating energy storage devices to DC microgrid," *IEEE Trans. Power Electron.*, vol. 35, no. 10, pp. 10501–10514, Oct. 2020.
[12] H. Matsuo, W. Lin, F. Kurokawa, T. Shigemizu, and N. Watanabe, "Characteristics of the multiple-input DC-DC converter," *IEEE Trans. Ind. Electron.*, vol. 51, no. 3, pp. 625–631, Jun. 2004.
[13] A. Vettuparambil, K. Chatterjee, and B. G. Fernandes, "A multiport converter interfacing solar photovoltaic modules and energy storage with DC microgrid," *IEEE Trans. Ind. Electron.*, vol. 68, no. 4, pp. 3113–3123, Apr. 2021.
[14] W. Wu, X. Wu, Y. Zhao, L. Wang, T. Zhao, and L. Jing, "An improved multiport DC power flow controller for VSC-MTDC grids," *IEEE Access*, vol. 8, pp. 7573–7586, 2020.
[15] Y.-M. Chen, Y.-C. Liu, and F.-Y. Wu, "Multi-input DC/DC converter based on the multiwinding transformer for renewable energy applications," *IEEE Trans. Ind. Appl.*, vol. 38, no. 4, pp. 1096–1104, Jul. 2002.
[16] J. L. Duarte, M. Hendrix, and M. G. Simoes, "Three-port bidirectional converter for hybrid fuel cell systems," *IEEE Trans. Power Electron.*, vol. 22, no. 2, pp. 480–487, Mar. 2007.
[17] D. Liu and H. Li, "A ZVS bi-directional DC–DC converter for multiple energy storage elements," *IEEE Trans. Power Electron.*, vol. 21, no. 5, pp. 1513–1517, Sep. 2006.
[18] V. N. S. R. Jakka, A. Shukla, and G. D. Demetriades, "Dual-transformer-based asymmetrical triple-port active bridge (DT-ATAB) isolated DC–DC converter," *IEEE Trans. Ind. Electron.*, vol. 64, no. 6, pp. 4549–4560, Jun. 2017.
[19] C. Zhao, S. D. Round, and J. W. Kolar, "An isolated three-port bidirectional DC-DC converter with decoupled power flow management," *IEEE Trans. Power Electron.*, vol. 23, no. 5, pp. 2443–2453, Sep. 2008.
[20] H. Qin and J. W. Kimball, "Generalized average modeling of dual active bridge DC–DC converter," *IEEE Trans. Power Electron.*, vol. 27, no. 4, pp. 2078–2084, Apr. 2012.
[21] J. A. Mueller and J. W. Kimball, "An improved generalized average model of DC–DC dual active bridge converters," *IEEE Trans. Power Electron.*, vol. 33, no. 11, pp. 9975–9988, Nov. 2018.
[22] Z. Li, Y. Wang, L. Shi, J. Huang, Y. Cui, and W. Lei, "Generalized averaging modeling and control strategy for three-phase dual-active-bridge DC-DC converters with three control variables," in *Proc. IEEE Appl. Power Electron. Conf. Expo. (APEC)*, Mar. 2017, pp. 1078–1084.
[23] J. Yang, G. Buticchi, C. Gu, S. Günter, H. Zhang, and P. Wheeler, "A generalized input impedance model of multiple active bridge converter," *IEEE Trans. Transport. Electrific.*, vol. 6, no. 4, pp. 1695–1706, Dec. 2020.
[24] R. Grino and A. Dòria-Cerezo, "Modelling and simulation of a magnetically coupled multiport DC-DC converter," in *Proc. 24th IEEE Int. Conf. Emerg. Technol. Factory Autom. (ETFA)*, Sep. 2019, pp. 481–487.
[25] H. Pinheiro and P. K. Jain, "Series-parallel resonant UPS with capacitive output DC bus filter for powering HFC networks," *IEEE Trans. Power Electron.*, vol. 17, no. 6, pp. 971–979, Nov. 2002.
[26] E. S. Oluwasogo and H. Cha, "Self-current sharing in dual-transformer-based triple-port active bridge DC–DC converter with reduced device count," *IEEE Trans. Power Electron.*, vol. 36, no. 5, pp. 5290–5301, May 2021.
[27] G. Buticchi, L. F. Costa, D. Barater, M. Liserre, and E. D. Amarillo, "A quadruple active bridge converter for the storage integration on the more electric aircraft," *IEEE Trans. Power Electron.*, vol. 33, no. 9, pp. 8174–8186, Sep. 2018.

[28] K. Xiangli, S. Li, and K. M. Smedley, "Decoupled PWM plus phase-shift control for a dual-half-bridge bidirectional DC–DC converter," *IEEE Trans. Power Electron.*, vol. 33, no. 8, pp. 7203–7213, Aug. 2018.
[29] I. Biswas, D. Kastha, and P. Bajpai, "Small signal modeling and decoupled controller design for a triple active bridge multiport DC–DC converter," *IEEE Trans. Power Electron.*, vol. 36, no. 2, pp. 1856–1869, Feb. 2021.
[30] B. Choi, W. Lim, S. Choi, and J. Sun, "Comparative performance evaluation of current-mode control schemes adapted to asymmetrically driven bridge-type pulsewidth modulated DC-to-DC converters," *IEEE Trans. Ind. Electron.*, vol. 55, no. 5, pp. 2033–2042, May 2008.
[31] Z. Qian, O. Abdel-Rahman, H. Al-Atrash, and I. Batarseh, "Modeling and control of three-port DC/DC converter interface for satellite applications," *IEEE Trans. Power Electron.*, vol. 25, no. 3, pp. 637–649, Mar. 2010.
[32] M. Cupelli, S. K. Gurumurthy, and A. Monti, "Modelling and control of single phase DAB based MVDC shipboard power system," in *Proc. 43rd Annu. Conf. IEEE Ind. Electron. Soc. (IECON)*, Oct. 2017, pp. 6813–6819.
[33] S. K. Gurumurthy, M. Cupelli, and A. Monti, "State space modelling and control of triple phase shift modulated single phase DAB for shipboard power system," in *Proc. 43rd Annu. Conf. IEEE Ind. Electron. Soc. (IECON)*, Oct. 2017, pp. 6826–6832.
[34] M. Cupelli, S. K. Gurumurthy, S. K. Bhanderi, Z. Yang, P. Joebges, A. Monti, and R. W. De Doncker, "Port controlled Hamiltonian modeling and IDA-PBC control of dual active bridge converters for DC microgrids," *IEEE Trans. on Ind. Electron.*, vol. 66, no. 11, pp. 9065–9074, Mar. 2019.
[35] R. V. Meshram, M. Bhagwat, S. Khade, S. R. Wagh, A. M. Stankovic, and N. M. Singh, "Port-controlled phasor Hamiltonian modeling and IDA-PBC control of solid-state transformer," *IEEE Trans. Control Syst. Technol.*, vol. 27, no. 1, pp. 161–173, Nov. 2019.
[36] J. M. Olm, E. Fossas, V. Repecho, A. Dòria-Cerezo, and R. Grino, "Adaptive control-based voltage regulation of a magnetically coupled multiport DC-DC converter for electrified vehicles applications," in *Proc. IEEE Int. Symp. Circuits Syst. (ISCAS)*, Oct. 2020, pp. 1–5.
[37] J. M. Olm, E. Fossas, V. Repecho, A. Dòria-Cerezo, and R. Grino, "Feedback linearizing control of a magnetically coupled multiport DC-DC converter for automotive applications," in *Proc. 45th Annu. Conf. IEEE Ind. Electron. Soc. (IECON)*, Oct. 2019, pp. 2688–2692.
[38] A. Rosen, "A new network theorem," *J. Inst. Electr. Eng.*, vol. 62, no. 335, pp. 916–918, Nov. 1924.
[39] M. N. Kheraluwala, R. W. Gascoigne, D. M. Divan, and E. D. Baumann, "Performance characterization of a high-power dual active bridge DC-to-DC converter," *IEEE Trans. Ind. Appl.*, vol. 28, no. 6, pp. 1294–1301, Nov. 1992.
[40] G. Perica, "Elimination of leakage effects related to the use of windings with fractions of turns," *IEEE Trans. Power Electron.*, vol. PE-1, no. 1, pp. 39–47, Jan. 1986.

VICTOR REPECHO received the B.S., M.S., and Ph.D. degrees in electronic engineering from the Universitat Politècnica de Catalunya (UPC), Barcelona, Spain, in 2006, 2012, and 2018, respectively. Since 2010, he has been a Development Engineer with the Institute of Industrial and Control Engineering (IOC), UPC. Since 2019, he has been an Assistant Professor with the Automatic Control Department, UPC. His research interests include digital control, nonlinear control, and control of power electronic converters.

JOSEP M. OLM received the M.S. and Ph.D. degrees in physics from the University of Barcelona, Barcelona, Spain, in 1989, and the Universitat Politècnica de Catalunya, Barcelona, in 2004.

Since 2003, he has been with the Universitat Politècnica de Catalunya, where he is currently an Associate Professor with the Department of Mathematics and a Researcher with the Institute of Industrial and Control Engineering. His research interests include control theory, including sliding, adaptive, repetitive, and complex networks control. He is the author or coauthor of more than 80 journal articles and conference papers, and one book.

Dr. Olm served as an Associate Editor for the IEEE TRANSACTIONS ON CIRCUITS AND SYSTEMS-I: REGULAR PAPERS, from 2014 to 2015.

ROBERT GRIÑÓ (Senior Member, IEEE) received the M.Sc. degree in electrical engineering and the Ph.D. degree in automatic control from the Universitat Politècnica de Catalunya (UPC), Barcelona, Spain, in 1989 and 1997, respectively.

From 1990 to 1991, he was a Research Assistant with the Instituto de Cibernética, UPC. From 1992 to 1998, he was an Assistant Professor with the Automatic Control Department, UPC, where he has been an Associate Professor since 1998. He is currently the Director of the Institute of Industrial and Control Engineering (IOC), UPC. His research interests include digital control, nonlinear control, and control of power electronic converters.

Dr. Griñó is a member of the Spanish Committee of Automatica (CEA-IFAC) and an affiliate of the International Federation of Automatic Control (IFAC) and member of its Technical Committee 6.3, Power and Energy Systems.

ARNAU DÒRIA-CEREZO was born in Barcelona, Spain, in 1974. He received the bachelor's degree in electromechanical engineering from the Universitat Politècnica de Catalunya (UPC), Barcelona, in 2001, the D.E.A. degree in industrial automation from the Institut National des Sciences Appliqueés de Lyon, Villeurbanne, France, in 2001, and the Ph.D. degree in advanced automation and robotics from UPC, in 2006.

He is currently an Associate Professor with the Department of Electrical Engineering, UPC, and carries on his research activities with the Advanced Control of Energy Systems Group, the Institute of Industrial and Control Engineering, UPC. From 2003 to 2004, he was a Control Training Site-Research Fellow with the Laboratoire des Signaux et Systèmes, Supélec, France. He was a Visitor with the Technische Universiteit Delft, Delft, The Netherlands, in 2010. His research interests include modeling and control of electrical systems, and automotive applications.

Dr. Dòria-Cerezo has been an Associate Editor of *Control Engineering Practice*, since 2017.

ENRIC FOSSAS (Senior Member, IEEE) received the Graduate and Ph.D. degrees in mathematics from the Universitat de Barcelona, in 1981 and 1986, respectively.

Since 1981, he taught mathematics with the Universitat de Barcelona, and mathematics and automatic control with the Universitat Politècnica de Catalunya (UPC), where he is currently employed as a Full Professor. He worked as the Head of the Department of Applied Mathematics, UPC, from September 1993 to August 1999, the Director of the Institute of Industrial and Control Engineering, UPC, from July 2003 to July 2009, and the Rector of UPC, from November 2013 to November 2017. His research interests include piecewise continuous systems, variable structure systems, and nonlinear control with applications to power electronics.